Journal of Zhejiang University-SCIENCE C (Computers & Electronics)
ISSN 1869-1951 (Print); ISSN 1869-196X (Online)
www.zju.edu.cn/jzus; www.springerlink.com
E-mail: jzus@zju.edu.cn

Nonlinear path-following method for fixed-wing unmanned aerial vehicles*

Jia-ming ZHANG†1, Qing LI[1], Nong CHENG[1,2], Bin LIANG[1]

([1]*Department of Automation, Tsinghua University, Beijing 100084, China*)

([2]*Science and Technology on Aircraft Control Laboratory, Flight Automatic Control Research Institute, Xi'an 710065, China*)

†E-mail: zhangjm09@mails.tsinghua.edu.cn

Received June 15, 2012; Revision accepted Dec. 19, 2012; Crosschecked Jan. 16, 2013

Abstract: A path-following method for fixed-wing unmanned aerial vehicles (UAVs) is presented in this paper. This method consists of an outer guidance loop and an inner control loop. The guidance law relies on the idea of tracking a virtual target. The motion of the virtual target is explicitly specified. The main advantage of this guidance law is that it considers the maneuvering ability of the aircraft. The aircraft can asymptotically approach the defined path with smooth movements. Meanwhile, the aircraft can anticipate the upcoming transition of the flight path. Moreover, the inner adaptive flight control loop based on attractive manifolds can follow the command generated by the outer guidance loop. This adaptive control law introduces a first-order filter to avoid solving the partial differential equation in the immersion and invariance adaptive control. The performance of the proposed path-following method is validated by the numerical simulation.

Key words: Path following, Virtual target, Flight control, Unmanned aerial vehicle (UAV)
doi:10.1631/jzus.C1200195 **Document code:** A **CLC number:** V24

1 Introduction

Unmanned aerial vehicles (UAVs) can be widely used to inspect piecewise linear infrastructures, such as oil-gas pipelines, roads, and power-lines (Rathinam *et al*., 2005; Holt and Beard, 2010; Bruggemann *et al*., 2011). Therefore, it is critical for UAVs to follow the 2D piecewise linear path specified by waypoints.

This paper makes use of the typical cascade control strategy that separates the path-following problem into an outer guidance loop and an inner control loop (Raffo *et al*., 2010; Cichella *et al*., 2011). The guidance loop directs the aircraft to the desired path and the control loop follows the command generated by the outer loop. The outer and inner loops can be designed separately.

The classic guidance law is based on a proportional-integral-derivative (PID) linear controller. However, this method is not effective when the aircraft is far away from the defined path. A path-following method using a virtual reference vehicle is proposed in the robotics area (Coulter, 1992; Normey-Rico *et al*., 1999; Raffo *et al*., 2009). The virtual robot that has the same kinematic model as the real robot is assumed over the desired trajectory. The objective is to find the control input to drive the error between the real robot and the virtual reference robot to the origin to follow the desired path. This method can be used to solve the path-following problem for UAVs (Cichella *et al*., 2011; Raffo *et al*., 2011).

Niculescu (2001) proposed the guidance law based on a virtual target for UAVs. In this method, the virtual target is assumed as a virtual point, rather than a virtual reference vehicle and the aircraft points to the virtual point directly. This nonlinear guidance law can accommodate large deviations from straight paths. This guidance method is adapted by assuming that the

* Project supported by the Aeronautical Science Foundation of China (Nos. 20100758002 and 20128058006) and the National Natural Science Foundation of China (No. 61174168)
© Zhejiang University and Springer-Verlag Berlin Heidelberg 2013

virtual target moves along the path with a fixed distance before the aircraft (Park *et al*., 2007). However, the speed of the virtual target is not explicit in this method. The motion of the virtual target can be related to that of the aircraft in the guidance law proposed by Medagoda and Gibbens (2010). However, the stability of this method is not analyzed. Gates (2010) indirectly determined the motion of the virtual target by introducing fictitious forces that comprise a spring-like force and a drag force between the vehicle and the virtual target. However, this method is too complicated.

The method in this paper also involves a virtual point. In this method, the speed of the virtual target is explicitly determined and related to that of the real vehicle. The aircraft adapts its heading to track the virtual target accordingly and approaches the desired path with smooth movements. This can reduce the command for the inner control loop by taking into account the turning ability of the aircraft. In this method, the aircraft always runs after the virtual target, even if the aircraft flies along the desired path. If the flight path changes its direction suddenly, the aircraft can adapt its heading before reaching the transition point of the flight path to track the virtual target, which avoids the acute heading change. In particular, this method is very simple.

The inner adaptive flight control loop is designed to follow the command generated by the outer guidance loop. Traditionally, the linear flight controllers are designed at multiple trimmed flight conditions and combined using gain scheduling to guarantee the performance in the entire flight envelope. However, this process requires extensive offline analysis and flight testing. The well-known feedback linearization approach has been proposed to overcome the shortcoming of linear design approaches (Snell *et al.*, 1992). However, one problem with this method is that it requires an accurate aircraft mathematical model. This is generally impossible, because it is rather difficult to exactly model the aerodynamic characteristics. To overcome this problem, the adaptive feedback linearization method based on neural networks has been developed to compensate for uncertainties in the aircraft model (Shin and Calise, 2008). However, the dynamics of the estimation error cannot be directly prescribed, which may cause the undesired transient response of the closed-loop system.

Recently, an immersion and invariance (I&I) adaptive control has been proposed for uncertain nonlinear systems (Astolfi and Ortega, 2003). This method allows for prescribing the dynamics of the parameter estimation error. After the parameter estimate happens to converge to its corresponding true value, the adaptive parameter estimation process automatically stops and the dynamics of the closed-loop system relies on attractive manifolds that are independent of unknown parameters. However, this method relies on the solution of a partial differential equation (PDE), which becomes difficult for multivariable systems.

To overcome the problem of solving the PDE, a modification of the I&I adaptive control method has been developed (Seo and Akella, 2008; 2009). This adaptive control method is based on attractive manifolds and involves a first-order filter to sidestep solving the PDE. This method has been applied to robot manipulator control (Seo and Akella, 2008) and spacecraft attitude-tracking control (Seo and Akella, 2009). In this paper, the adaptive flight control law based on attractive manifolds has been derived for UAVs to follow the reference command.

2 Guidance law

The basic idea of the guidance law based on a virtual target is shown in Fig. 1. The flight path is specified by waypoints 1 and 2. Initially, the aircraft deviates from the path and begins to adapt its heading to track the virtual target to follow the path. Meanwhile, the virtual target starts to move along the defined path from the intersection point *C* of the heading of the aircraft and the flight path.

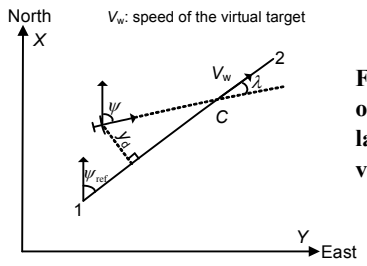

Fig. 1 Illustration of the guidance law based on a virtual target

In Fig. 1, the difference angle λ between the real aircraft heading ψ and the reference heading ψ_{ref} is derived as

$$\lambda=\psi-\psi_{\text{ref}}. \tag{1}$$

The dynamics of λ can be derived as

$$\dot{\lambda}=\dot{\psi}=-V_{\text{w}}\sin\lambda/R, \tag{2}$$

where R represents the distance between the aircraft and the virtual target, and the speed of the virtual target V_{w} is explicitly selected as

$$V_{\text{w}}=V\cos\lambda, \tag{3}$$

where V represents the aircraft speed. It can be found that the speed of the virtual target is equal to the projection of the aircraft speed on the defined path. Therefore, the aircraft runs after the virtual target.

Define the following Lyapunov function as

$$V_1=\frac{1}{2}\lambda^2. \tag{4}$$

Differentiating V_1 and using Eq. (3) give

$$\dot{V}_1=\lambda\dot{\lambda}=-\frac{V_{\text{w}}\sin\lambda}{R}\lambda=-\frac{V\cos\lambda\sin\lambda}{R}\lambda.$$

It is obvious that $\lambda\sin\lambda$ is non-negative, assuming that $-\pi/2<\lambda<\pi/2$. Therefore, it can be found that $\dot{V}_1\le 0$. By virtue of Barbalat's lemma, it can be concluded that

$$\lim_{t\to\infty}\lambda=0. \tag{5}$$

According to Eqs. (1) and (5), it can be found that

$$\lim_{t\to\infty}\psi=\psi_{\text{ref}}. \tag{6}$$

Therefore, the heading of the aircraft asymptotically follows the reference heading. Meanwhile, it can be derived that

$$y_{\text{d}}=R\sin\lambda, \tag{7}$$

where y_{d} represents the lateral displacement between the aircraft and the path. According to Eqs. (5) and (7), it can be concluded that

$$\lim_{t\to\infty}y_{\text{d}}=0. \tag{8}$$

Therefore, the aircraft approaches the desired flight path asymptotically with smooth movements, which reduces the command for the inner control loop. Once the aircraft flies on the desired path, according to Eq. (3), it can be found that

$$V_{\text{w}}=V. \tag{9}$$

This constraint implies that the speed of the virtual target is equal to the aircraft speed. Therefore, the aircraft still pursues the virtual target, even if the aircraft flies on the desired path. If the flight path changes its direction suddenly, the virtual target can transit to the next flight path before the aircraft. The aircraft adapts its heading before arriving at the transition point of the flight path to track the virtual target, which avoids the acute heading command. Additionally, this guidance law behaves as a closed-loop system, because the aircraft always tracks the virtual target accordingly and the motion of the virtual target is related to that of the aircraft. Therefore, this method is insensitive to the wind disturbance.

The instantaneous position of the virtual target can be calculated as

$$\begin{bmatrix}X_{\text{w}}\\Y_{\text{w}}\end{bmatrix}_i=\begin{bmatrix}X_{\text{w}}\\Y_{\text{w}}\end{bmatrix}_{i-1}+V_{\text{w}}\begin{bmatrix}\cos\psi_{\text{ref}}\\\sin\psi_{\text{ref}}\end{bmatrix}\Delta T, \tag{10}$$

where X_{w} and Y_{w} represent the position of the moving virtual target, and ΔT is the integration time. To track the virtual target, the heading angle command ψ_{com} can be calculated as

$$\psi_{\text{com}}=\arctan(\Delta_y/\Delta_x), \tag{11}$$

where $\Delta_x=X_w-X_a$, $\Delta_y=Y_w-Y_a$, and X_{a} and Y_{a} represent the position of the aircraft.

The aircraft uses angular rates as the control input to change its heading. Using the proportional controller, the roll angle command ϕ_{com} can be derived as

$$\phi_{\text{com}}=k_\psi(\psi_{\text{com}}-\psi). \tag{12}$$

Then, the roll angular rate command p_{com} is determined as

$$p_{\text{com}}=k_{\phi}(\phi_{\text{com}}-\phi). \tag{13}$$

To perform the coordinated turn, the yaw rate can be used as the control input, and the yaw angular rate command r_{com} is determined as

$$r_{\text{com}}=k_{\beta}(\beta_{\text{com}}-\beta), \tag{14}$$

where the sideslip angle command β_{com} is kept at zero to avoid sideslip. The angular rate command can be followed by the inner adaptive flight control law based on attractive manifolds proposed in Section 3.

3 Adaptive flight control law

3.1 Aircraft dynamics

The aircraft is a fixed-wing UAV developed by Eidgenössische Technische Hochschule (ETH) Zürich (Switzerland). The nonlinear dynamic equations of the aircraft can be written as (Shin and Kim, 2004)

$$\begin{cases} \dot{p}=(c_1 r+c_2 p)q+c_3 L+c_4 N, \\ \dot{q}=c_5 pr-c_6(p^2-r^2)+c_7 M, \\ \dot{r}=(c_8 p-c_2 r)q+c_4 L+c_9 N, \end{cases} \tag{15}$$

where p, q, and r represent the roll, pitch, and yaw angular rate, respectively. The moment of inertia components are defined as

$$\begin{aligned} &\Gamma c_1=(I_y-I_z)I_z-I_{xz}^2,\ \Gamma c_2=(I_x-I_y+I_z)I_{xz}, \\ &\Gamma c_3=I_z,\ \Gamma c_4=I_{xz},\ c_5=(I_z-I_x)/I_y,\ c_6=I_{xz}/I_y, \\ &c_7=1/I_y,\ \Gamma c_8=I_x(I_x-I_y)+I_{xz}^2,\ \Gamma c_9=I_x, \end{aligned}$$

with $\Gamma=I_x I_z-I_{xz}^2$. The roll, pitch, and yaw moment can be expressed as a linear combination of state elements and control surface deflections (Ducard and Geering, 2008b):

$$\begin{cases} L=\bar{q}Sb(C_{La}\delta_a+C_{Le}\delta_e+C_{Lp}\tilde{p}+C_{Lr}\tilde{r}+C_{L\beta}\beta), \\ M=\bar{q}S\bar{c}(C_{Ma}\delta_a+C_{Me}\delta_e+C_{Mq}\tilde{q}+C_{M\alpha}\alpha), \\ N=\bar{q}Sb(C_{N\delta_r}\delta_r+C_{Nr}\tilde{r}+C_{N\beta}\beta), \end{cases} \tag{16}$$

where $\bar{q}$ is the dynamic pressure, S is the reference wing area, b is the reference wing span, $\bar{c}$ is the reference mean aerodynamic chord, δ_{a}, δ_{e}, and δ_{r} are the aileron, elevator, and rudder deflection, respectively, α is the angle of attack, and β is the sideslip angle. The terms C_{La}, C_{Le}, C_{Ma}, C_{Me}, and $C_{N\delta_r}$ are the control effectiveness coefficients and the terms C_{Lp}, C_{Lr}, $C_{L\beta}$, C_{Mq}, $C_{M\alpha}$, C_{Nr}, and $C_{N\beta}$ are the stability derivatives in the aerodynamic moments. The dimensionless angular rates $\tilde{p}$, $\tilde{q}$, and $\tilde{r}$ are defined as

$$\tilde{p}=\frac{bp}{2V},\quad \tilde{q}=\frac{\bar{c}q}{2V},\quad \tilde{r}=\frac{br}{2V}, \tag{17}$$

where V represents the aircraft speed. The detailed data about the aircraft model can be obtained from Ducard and Geering (2008b).

3.2 Adaptive flight control law

Substituting Eq. (16) into Eq. (15) and defining the state variable $\boldsymbol{x}=[p\ q\ r]^{\text{T}}$ and the control input $\boldsymbol{u}=[\delta_e\ \delta_a\ \delta_r]^{\text{T}}$ yield

$$\dot{\boldsymbol{x}}=\boldsymbol{f}(\boldsymbol{x})+\boldsymbol{\Phi}(\boldsymbol{x})\boldsymbol{\theta}+\boldsymbol{G}\boldsymbol{u}, \tag{18}$$

where

$$\boldsymbol{f}(\boldsymbol{x})=\begin{bmatrix} (c_1 r+c_2 p)q \\ c_5 pr-c_6(p^2-r^2) \\ (c_8 p-c_2 r)q \end{bmatrix},$$

$$\boldsymbol{\Phi}(\boldsymbol{x})=\bar{q}S\begin{bmatrix} bc_3\tilde{p} & bc_3\tilde{r} & bc_3\beta & 0 & 0 & bc_4\tilde{r} & bc_4\beta \\ 0 & 0 & 0 & \bar{c}c_7\tilde{q} & \bar{c}c_7\alpha & 0 & 0 \\ bc_4\tilde{p} & bc_4\tilde{r} & bc_4\beta & 0 & 0 & bc_9\tilde{r} & bc_9\beta \end{bmatrix},$$

$$\boldsymbol{G}=\bar{q}S\begin{bmatrix} c_3 bC_{Le} & c_3 bC_{La} & c_4 bC_{N\delta_r} \\ c_7\bar{c}C_{Me} & c_7\bar{c}C_{Ma} & 0 \\ c_4 bC_{Le} & c_4 bC_{La} & c_9 bC_{N\delta_r} \end{bmatrix},$$

$$\boldsymbol{\theta}=[C_{Lp}\quad C_{Lr}\quad C_{L\beta}\quad C_{Mq}\quad C_{M\alpha}\quad C_{Nr}\quad C_{N\beta}].$$

To track the reference command $\boldsymbol{x}_{\text{d}}=[p_{\text{d}}\ q_{\text{d}}\ r_{\text{d}}]^{\text{T}}$, we define the tracking error as

$$\boldsymbol{z}=\boldsymbol{x}-\boldsymbol{x}_{\text{d}}. \tag{19}$$

Differentiating Eq. (19) and using Eq. (18) give

$$\dot{\boldsymbol{z}} = \boldsymbol{h} + \boldsymbol{\Phi\theta} + \boldsymbol{v}_{\mathrm{c}}, \tag{20}$$

where the signals $\boldsymbol{h}$ and $\boldsymbol{v}_{\mathrm{c}}$ are defined as

$$\boldsymbol{h} = \boldsymbol{f} - \dot{\boldsymbol{x}}_{\mathrm{d}}, \tag{21}$$

$$\boldsymbol{v}_{\mathrm{c}} = \boldsymbol{Gu}. \tag{22}$$

To overcome the problem of solving the PDE, the filtered surface error is introduced using the first-order filter:

$$\dot{z}_{\mathrm{f}} = -az_{\mathrm{f}} + z, \tag{23}$$

where the time constant $a>0$. Moreover, we introduce the filtered signals:

$$\begin{cases} \dot{\boldsymbol{h}}_{\mathrm{f}} = -a\boldsymbol{h}_{\mathrm{f}} + \boldsymbol{h}, \\ \dot{\boldsymbol{\Phi}}_{\mathrm{f}} = -a\boldsymbol{\Phi}_{\mathrm{f}} + \boldsymbol{\Phi}, \\ \dot{\boldsymbol{v}}_{\mathrm{cf}} = -a\boldsymbol{v}_{\mathrm{cf}} + \boldsymbol{v}_{\mathrm{c}}. \end{cases} \tag{24}$$

Differentiating Eq. (23) and using Eq. (24), one has

$$\begin{aligned} \ddot{z}_{\mathrm{f}} &= -a\dot{z}_{\mathrm{f}} + \boldsymbol{h} + \boldsymbol{\Phi\theta} + \boldsymbol{v}_{\mathrm{c}} \\ &= -a\dot{z}_{\mathrm{f}} + (\dot{\boldsymbol{h}}_{\mathrm{f}} + a\boldsymbol{h}_{\mathrm{f}}) + (\dot{\boldsymbol{\Phi}}_{\mathrm{f}} + a\boldsymbol{\Phi}_{\mathrm{f}})\boldsymbol{\theta} + (\dot{\boldsymbol{v}}_{\mathrm{cf}} + a\boldsymbol{v}_{\mathrm{cf}}). \end{aligned} \tag{25}$$

Rearranging terms in Eq. (25) gives the following perfect differential:

$$\frac{\mathrm{d}(\dot{z}_{\mathrm{f}} - \boldsymbol{h}_{\mathrm{f}} - \boldsymbol{\Phi}_{\mathrm{f}}\boldsymbol{\theta} - \boldsymbol{v}_{\mathrm{cf}})}{\mathrm{d}t} = -a(\dot{z}_{\mathrm{f}} - \boldsymbol{h}_{\mathrm{f}} - \boldsymbol{\Phi}_{\mathrm{f}}\boldsymbol{\theta} - \boldsymbol{v}_{\mathrm{cf}}). \tag{26}$$

The solution of Eq. (26) is expressed as

$$\dot{z}_{\mathrm{f}} = \boldsymbol{h}_{\mathrm{f}} + \boldsymbol{\Phi}_{\mathrm{f}}\boldsymbol{\theta} + \boldsymbol{v}_{\mathrm{cf}} + \boldsymbol{\varepsilon}(t), \tag{27}$$

where $\boldsymbol{\varepsilon}(t)$ is the exponentially decaying term. The exponentially decaying signal $\boldsymbol{\varepsilon}(t)$ can be ignored in the stability analysis (Seo and Akella, 2008; 2009). Then, the filtered error dynamics can be expressed as

$$\dot{z}_{\mathrm{f}} = \boldsymbol{h}_{\mathrm{f}} + \boldsymbol{\Phi}_{\mathrm{f}}\boldsymbol{\theta} + \boldsymbol{v}_{\mathrm{cf}}. \tag{28}$$

In view of Eq. (28), the stabilizing signal $\boldsymbol{v}_{\mathrm{cf}}$ is specified as

$$\boldsymbol{v}_{\mathrm{cf}} = -\boldsymbol{h}_{\mathrm{f}} - \boldsymbol{\Phi}_{\mathrm{f}}\hat{\boldsymbol{\theta}} - kz_{\mathrm{f}} = -\boldsymbol{h}_{\mathrm{f}} - \boldsymbol{\Phi}_{\mathrm{f}}(\boldsymbol{\xi} + \boldsymbol{\eta}) - kz_{\mathrm{f}}, \tag{29}$$

where $\hat{\boldsymbol{\theta}}$ is the estimate of the unknown parameter vector $\boldsymbol{\theta}$. Different from the traditional parameter estimation method, the estimate based on attractive manifolds includes a partial estimate $\boldsymbol{\xi}$ and a nonlinear function $\boldsymbol{\eta}$. The nonlinear function $\boldsymbol{\eta}$ is selected as

$$\boldsymbol{\eta} = \gamma\boldsymbol{\Phi}_{\mathrm{f}}^{\mathrm{T}} z_{\mathrm{f}}, \tag{30}$$

where $\gamma>0$. The update law of $\boldsymbol{\xi}$ is selected as

$$\dot{\boldsymbol{\xi}} = -\gamma(-a\boldsymbol{\Phi}_{\mathrm{f}} + \boldsymbol{\Phi})^{\mathrm{T}} z_{\mathrm{f}} + \gamma\boldsymbol{\Phi}_{\mathrm{f}}^{\mathrm{T}} kz_{\mathrm{f}}, \tag{31}$$

where $k>0$. Substituting Eq. (29) into Eq. (28) gives

$$\dot{z}_{\mathrm{f}} = -\boldsymbol{\Phi}_{\mathrm{f}}(\boldsymbol{\xi} + \boldsymbol{\eta} - \boldsymbol{\theta}) - kz_{\mathrm{f}}. \tag{32}$$

The parameter estimation error is defined as

$$\boldsymbol{e} = \hat{\boldsymbol{\theta}} - \boldsymbol{\theta} = \boldsymbol{\xi} + \boldsymbol{\eta} - \boldsymbol{\theta}. \tag{33}$$

Then, Eq. (32) can be expressed as

$$\dot{z}_{\mathrm{f}} = -\boldsymbol{\Phi}_{\mathrm{f}}\boldsymbol{e} - kz_{\mathrm{f}}. \tag{34}$$

Differentiating Eq. (33) and using Eqs. (30), (31), and (34) yield

$$\begin{aligned} \dot{\boldsymbol{e}} &= \dot{\boldsymbol{\xi}} + \dot{\boldsymbol{\eta}} \\ &= -\gamma(-a\boldsymbol{\Phi}_{\mathrm{f}} + \boldsymbol{\Phi})^{\mathrm{T}} z_{\mathrm{f}} + \gamma\boldsymbol{\Phi}_{\mathrm{f}}^{\mathrm{T}} kz_{\mathrm{f}} + \gamma\dot{\boldsymbol{\Phi}}_{\mathrm{f}}^{\mathrm{T}} z_{\mathrm{f}} + \gamma\boldsymbol{\Phi}_{\mathrm{f}}^{\mathrm{T}}\dot{z}_{\mathrm{f}} \\ &= -\gamma(-a\boldsymbol{\Phi}_{\mathrm{f}} + \boldsymbol{\Phi})^{\mathrm{T}} z_{\mathrm{f}} + \gamma\boldsymbol{\Phi}_{\mathrm{f}}^{\mathrm{T}} kz_{\mathrm{f}} + \gamma(-a\boldsymbol{\Phi}_{\mathrm{f}} + \boldsymbol{\Phi})^{\mathrm{T}} z_{\mathrm{f}} \\ &\quad + \gamma\boldsymbol{\Phi}_{\mathrm{f}}^{\mathrm{T}}(-\boldsymbol{\Phi}_{\mathrm{f}}\boldsymbol{e} - kz_{\mathrm{f}}) \\ &= -\gamma\boldsymbol{\Phi}_{\mathrm{f}}^{\mathrm{T}}\boldsymbol{\Phi}_{\mathrm{f}}\boldsymbol{e}. \end{aligned} \tag{35}$$

According to Eq. (24), the control signal $\boldsymbol{v}_{\mathrm{c}}$ is determined as

$$\begin{aligned} \boldsymbol{v}_{\mathrm{c}} &= \dot{\boldsymbol{v}}_{\mathrm{cf}} + a\boldsymbol{v}_{\mathrm{cf}} \\ &= -\dot{\boldsymbol{h}}_{\mathrm{f}} - \dot{\boldsymbol{\Phi}}_{\mathrm{f}}(\boldsymbol{\xi} + \boldsymbol{\eta}) - \boldsymbol{\Phi}_{\mathrm{f}}(\dot{\boldsymbol{\xi}} + \dot{\boldsymbol{\eta}}) - k\dot{z}_{\mathrm{f}} \\ &\quad - a\boldsymbol{h}_{\mathrm{f}} - a\boldsymbol{\Phi}_{\mathrm{f}}(\boldsymbol{\xi} + \boldsymbol{\eta}) - akz_{\mathrm{f}} \\ &= -\boldsymbol{h} - \boldsymbol{\Phi}(\boldsymbol{\xi} + \boldsymbol{\eta}) - kz - \boldsymbol{\Phi}_{\mathrm{f}}(\dot{\boldsymbol{\xi}} + \dot{\boldsymbol{\eta}}). \end{aligned} \tag{36}$$

Substituting Eqs. (24), (30), and (31) into Eq. (36) gives

$$\begin{aligned}\boldsymbol{v}_{\mathrm{c}} &= -\boldsymbol{h} - \boldsymbol{\Phi}(\boldsymbol{\xi}+\boldsymbol{\eta}) - k\boldsymbol{z} - \boldsymbol{\Phi}_{\mathrm{f}}[-\gamma(-a\boldsymbol{\Phi}_{\mathrm{f}}+\boldsymbol{\Phi})^{\mathrm{T}}\boldsymbol{z}_{\mathrm{f}} \\ &\quad + \gamma\boldsymbol{\Phi}_{\mathrm{f}}^{\mathrm{T}}k\boldsymbol{z}_{\mathrm{f}} + \gamma(-a\boldsymbol{\Phi}_{\mathrm{f}}+\boldsymbol{\Phi})^{\mathrm{T}}\boldsymbol{z}_{\mathrm{f}} + \gamma\boldsymbol{\Phi}_{\mathrm{f}}^{\mathrm{T}}(-a\boldsymbol{z}_{\mathrm{f}}+\boldsymbol{z})] \\ &= -\boldsymbol{f} - \boldsymbol{\Phi}(\boldsymbol{\xi}+\boldsymbol{\eta}) - k\boldsymbol{z} - \gamma\boldsymbol{\Phi}_{\mathrm{f}}\boldsymbol{\Phi}_{\mathrm{f}}^{\mathrm{T}}[(k-a)\boldsymbol{z}_{\mathrm{f}}+\boldsymbol{z}] + \dot{\boldsymbol{x}}_{\mathrm{d}}.\end{aligned} \tag{37}$$

By the definition of $\boldsymbol{v}_{\mathrm{c}}$, the control signal $\boldsymbol{u}$ can be determined as

$$\begin{aligned}\boldsymbol{u} = \boldsymbol{G}^{-1}\boldsymbol{v}_{\mathrm{c}} = \boldsymbol{G}^{-1}\big(&-\boldsymbol{f} - \boldsymbol{\Phi}(\boldsymbol{\xi}+\boldsymbol{\eta}) - k\boldsymbol{z} \\ &-\gamma\boldsymbol{\Phi}_{\mathrm{f}}\boldsymbol{\Phi}_{\mathrm{f}}^{\mathrm{T}}\big((k-a)\boldsymbol{z}_{\mathrm{f}}+\boldsymbol{z}\big) + \dot{\boldsymbol{x}}_{\mathrm{d}}\big).\end{aligned} \tag{38}$$

The input matrix $\boldsymbol{G}$ is invertible for all cases, because the control surface of the aircraft is designed to control each axis's angular rate of the aircraft independently (Shin and Kim, 2004).

Consider the following Lyapunov function:

$$V_2 = \frac{1}{2}\boldsymbol{z}_{\mathrm{f}}^{\mathrm{T}}\boldsymbol{z}_{\mathrm{f}} + \frac{1}{2}\gamma^{-1}\boldsymbol{e}^{\mathrm{T}}\boldsymbol{e}. \tag{39}$$

Differentiating Eq. (39) and using Eqs. (34) and (35) give

$$\begin{aligned}\dot{V}_2 &= \boldsymbol{z}_{\mathrm{f}}^{\mathrm{T}}(-\boldsymbol{\Phi}_{\mathrm{f}}\boldsymbol{e} - k\boldsymbol{z}_{\mathrm{f}}) + \gamma^{-1}\boldsymbol{e}^{\mathrm{T}}(-\gamma\boldsymbol{\Phi}_{\mathrm{f}}^{\mathrm{T}}\boldsymbol{\Phi}_{\mathrm{f}}\boldsymbol{e}) \\ &= -\boldsymbol{z}_{\mathrm{f}}^{\mathrm{T}}\boldsymbol{\Phi}_{\mathrm{f}}\boldsymbol{e} - k\|\boldsymbol{z}_{\mathrm{f}}\|^2 - \|\boldsymbol{\Phi}_{\mathrm{f}}\boldsymbol{e}\|^2.\end{aligned}$$

Using Young's inequality, one has

$$\left|\boldsymbol{z}_{\mathrm{f}}^{\mathrm{T}}\boldsymbol{\Phi}_{\mathrm{f}}\boldsymbol{e}\right| \le \frac{1}{2}\|\boldsymbol{z}_{\mathrm{f}}\|^2 + \frac{1}{2}\|\boldsymbol{\Phi}_{\mathrm{f}}\boldsymbol{e}\|^2. \tag{40}$$

Then, it can be found that

$$\dot{V}_2 \le -\left(k - \frac{1}{2}\right)\|\boldsymbol{z}_{\mathrm{f}}\|^2 - \frac{1}{2}\|\boldsymbol{\Phi}_{\mathrm{f}}\boldsymbol{e}\|^2. \tag{41}$$

If $k>0.5$, then $\dot{V}_2 \le 0$. By Barbalat's lemma, the following conclusion can be guaranteed:

$$\lim_{t\to\infty}[\boldsymbol{z}_{\mathrm{f}}(t), \boldsymbol{\Phi}_{\mathrm{f}}\boldsymbol{e}(t)] = 0. \tag{42}$$

Therefore, $\boldsymbol{z}_{\mathrm{f}}$ converges to zero. According to Eq. (23), it can be concluded that the error $\boldsymbol{z}$ converges to zero, which implies that the angular rate follows the command. Finally, the airspeed is kept constant using the method proposed by Ducard and Geering (2008a), which is not presented in this paper.

It can be found that the adaptive flight control law can improve the performance of the inner flight control loop, which yields that the inner control loop can follow the command generated by the outer guidance loop. Meanwhile, the proposed guidance law allows a reduction in the command for the inner control loop. Therefore, the closed-loop stability of the complete system can be guaranteed.

4 Numerical simulations

This section presents simulation results of the path-following logic applied to the full six-degree-of-freedom UAV model. The simulation is performed at the initial velocity of 25 m/s and an altitude of 500 m. The parameters in Eqs. (12), (13), and (14) are determined as k_{ψ}=2, k_{ϕ}=5, and k_{β}=−10. The parameters of the adaptive control law in Eqs. (23), (29), and (30) are selected as a=5, k=5, and γ=10.

In Fig. 2, the desired flight path initially changes direction 15° to the right, then 15° to the left. All lines of the defined flight path are maintained at a constant altitude. It can be seen that the aircraft can follow the defined flight path asymptotically. The aircraft can change its heading before reaching the transition point of the flight path, which avoids the acute heading change. In Fig. 3, it can be seen that the command of the heading angle is smooth. Fig. 4 shows the history of the roll angle that is reasonable. In Fig. 5, it can be seen that the aircraft can perform the bank-to-turn maneuver to follow the desired path. Figs. 6 and 7 show the history of the roll and the yaw angular rates, respectively. It can be found that the inner flight control loop can follow the command satisfactorily. Fig. 8 shows the aileron and rudder deflection, which are within the saturation limitation. Fig. 9 shows the performance of the path-following method with a steady 5 m/s crosswind from west to east. It can be seen that the aircraft still follows the desired flight path asymptotically after the initial transient decays. If the aircraft is pushed to diverge from the flight path due to the wind, the aircraft adapts its heading to track the virtual target to approach the defined path accordingly. This simulation demonstrates that the proposed path-following method is insensitive to the wind.

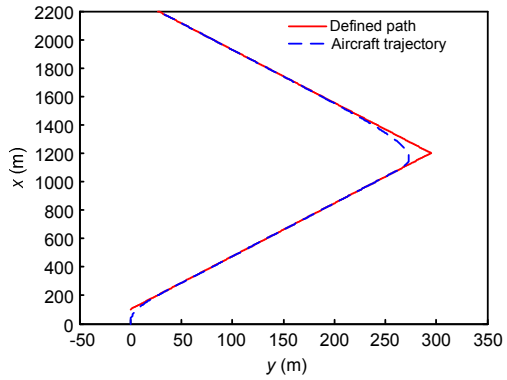

Fig. 2 Defined flight path and aircraft trajectory

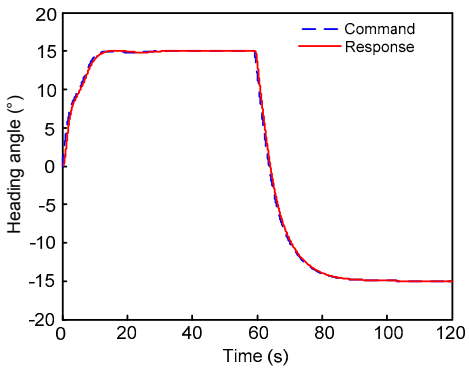

Fig. 3 Command of the heading angle and its response

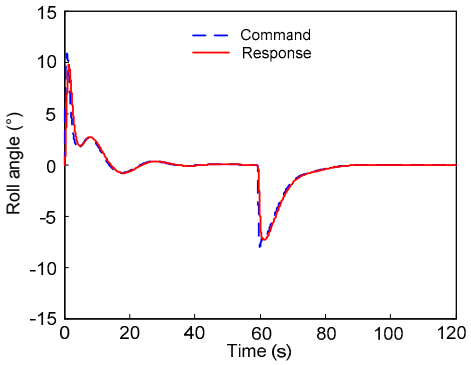

Fig. 4 Command of the roll angle and its response

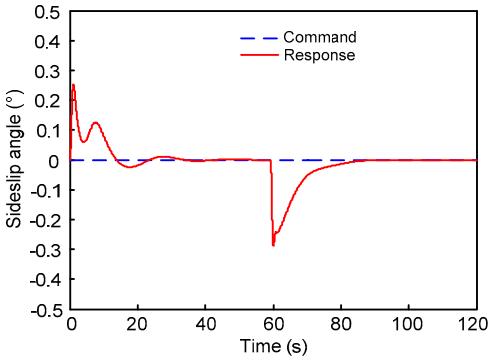

Fig. 5 Command of the sideslip angle and its response

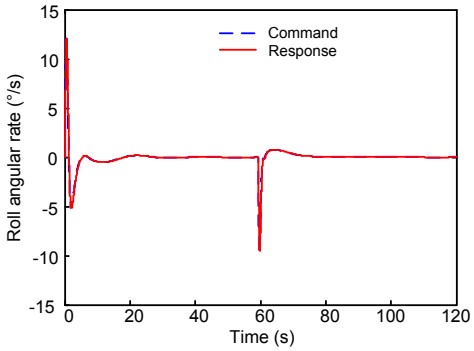

Fig. 6 Command of the roll angular rate and its response

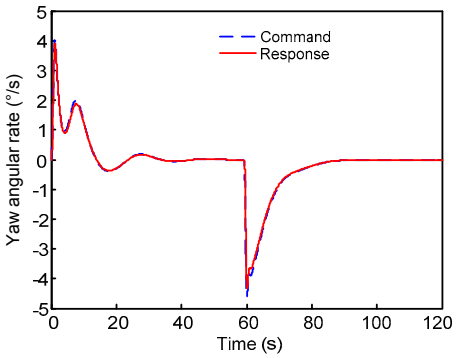

Fig. 7 Command of the yaw angular rate and its response

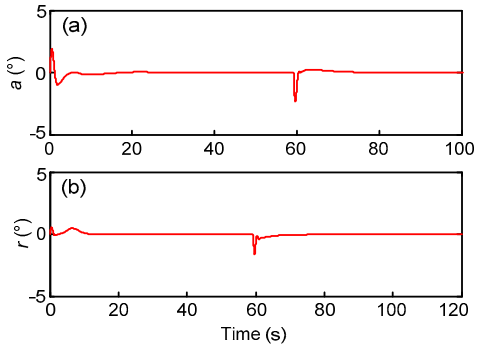

Fig. 8 History of the aileron (a) and rudder deflection (b)

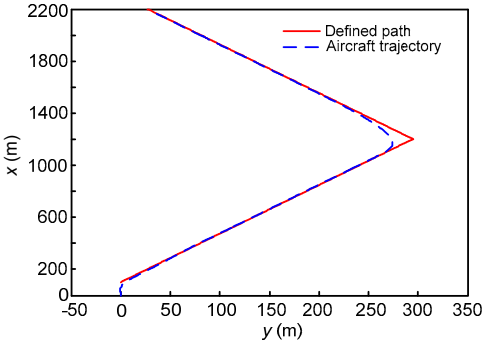

Fig. 9 Defined flight path and aircraft trajectory with wind

5 Conclusions

The main contribution of this paper is to propose a path-following method based on a virtual target for fixed-wing UAVs. This guidance law guarantees that the aircraft can approach the desired path with smooth movements, which reduces the command for the inner control loop. This method can also anticipate a sudden change of the flight path, which avoids the acute heading change. The second contribution of this paper is the proposal of the adaptive flight control law based on attractive manifolds. This adaptive control law relies on the idea of driving the dynamics of the parameter estimation error within attractive manifolds and introduces a linear filter for the regressor matrix to avoid solving the partial differential equations for the multivariable system. Numerical simulations illustrate the effectiveness of the proposed path-following method.

References

Astolfi, A., Ortega, R., 2003. Immersion and invariance: a new tool for stabilization and adaptive control of nonlinear systems. *IEEE Trans. Autom. Control*, **48**(4):590-606. [doi:10.1109/TAC.2003.809820]

Bruggemann, T.S., Ford, J.J., Walker, R.A., 2011. Control of aircraft for inspection of linear infrastructure. *IEEE Trans. Control Syst. Technol*., **19**(6):1397-1409. [doi:10.1109/TCST.2010.2093937]

Cichella, V., Xargay, E., Dobrokhodov, V., Kaminer, I., Pascoal, A.M., Hovakimyan, N., 2011. Geometric 3D Path-Following Control for a Fixed-Wing UAV on SO(3). AIAA Guidance, Navigation and Control Conf., No. AIAA-2011-6415.

Coulter, R.C., 1992. Implementation of the Pure Pursuit Path Tracking Algorithm. Technical Report No. CMU-RI-TR-92-01, Robotics Institute, Carnegie Mellon University.

Ducard, G., Geering, H., 2008a. Airspeed Control for Unmanned Aerial Vehicles: a Nonlinear Dynamic Inversion Approach. 16th Mediterranean Conf. on Control and Automation, p.676-681. [doi:10.1109/MED.2008.4602202]

Ducard, G., Geering, H., 2008b. Efficient nonlinear actuator fault detection and isolation system for unmanned aerial vehicles. *J. Guid. Control Dyn*., **31**(1):225-237. [doi:10.2514/1.31693]

Gates, D.J., 2010. Nonlinear path following method. *J. Guid. Control Dyn*., **33**(2):321-332. [doi:10.2514/1.46679]

Holt, R.S., Beard, R.W., 2010. Vision-based road-following using proportional navigation. *J. Intell. Rob. Syst*., **57**(1-4):193-216. [doi:10.1007/s10846-009-9353-7]

Medagoda, E.D.B., Gibbens, P.W., 2010. Synthetic-waypoint guidance algorithm for following a desired flight trajectory. *J. Guid. Control Dyn*., **33**(2):601-606. [doi:10.2514/1.46204]

Niculescu, M., 2001. Lateral Track Control for Aerosonde UAV. Proc. 39th AIAA Aerospace Sciences Meeting and Exhibit, No. AIAA-2001-0016.

Normey-Rico, J.E., Gómez-Ortega, J., Camacho, E.F., 1999. A Smith-predictor-based generalised predictive controller for mobile robot path-tracking. *Control Eng. Pract.*, **7**(6):729-740. [doi:10.1016/S0967-0661(99)00025-8]

Park, S., Deyst, J., How, J.P., 2007. Performance and Lyapunov stability of a nonlinear path-following guidance method. *J. Guid. Control Dyn*., **30**(6):1718-1728. [doi:10.2514/1.28957]

Raffo, G.V., Gomes, G.K., Normey-Rico, J.E., Kelber, C.R., Becker, L.B., 2009. A predictive controller for autonomous vehicle path tracking. *IEEE Trans. Intell. Transp. Syst*., **10**(1):92-102. [doi:10.1109/TITS.2008.2011697]

Raffo, G.V., Ortega, M.G., Rubio, F.R., 2010. An integral predictive/nonlinear H_∞ control structure for a quadrotor helicopter. *Automatica*, **46**(1):29-39. [doi:10.1016/j.automatica.2009.10.018]

Raffo, G.V., Ortega, M.G., Rubio, F.R., 2011. Path tracking of a UAV via an underactuated H_∞ control strategy. *Eur. J. Control*, **17**(2):194-213. [doi:10.3166/ejc.17.194-213]

Rathinam, S., Kim, Z.W., Soghikian, A., Sengupta, R., 2005. Vision Based Following of Locally Linear Structures Using an Unmanned Aerial Vehicle. 44th IEEE Conf. on Decision and Control, and European Control Conf., p.6085-6090. [doi:10.1109/CDC.2005.1583135]

Seo, D., Akella, M.R., 2008. High-performance spacecraft adaptive attitude-tracking control through attracting manifold design. *J. Guid. Control Dyn*., **31**(4):884-891. [doi:10.2514/1.33308]

Seo, D., Akella, M.R., 2009. Non-certainty equivalence adaptive control for robot manipulator systems. *Syst. Control Lett*., **58**(4):304-308. [doi:10.1016/j.systconle.2008.11.008]

Shin, D., Kim, Y., 2004. Reconfigurable flight control system design using adaptive neural networks. *IEEE Trans. Control Syst. Technol*., **12**(1):87-100. [doi:10.1109/TCST.2003.821957]

Shin, Y., Calise, A.J., 2008. Adaptive control of advanced fighter aircraft in nonlinear flight regimes. *J. Guid. Control Dyn*., **31**(5):1464-1477. [doi:10.2514/1.30213]

Snell, S., Enns, D., Garrard, W., 1992. Nonlinear inversion flight control for a supermaneuverable aircraft. *J. Guid. Control Dyn*., **15**(4):976-984. [doi:10.2514/3.20932]